Systems/Circuits

Gamma Synchrony Predicts Neuron–Neuron Correlations and Correlations with Motor Behavior in Extrastriate Visual Area MT

Joonyeol Lee and Stephen G. Lisberger
Howard Hughes Medical Institute and Department of Neurobiology, Duke University School of Medicine, Durham, North Carolina 27710

Correlated variability of neuronal responses is an important factor in estimating sensory parameters from a population response. Large correlations among neurons reduce the effective size of a neural population and increase the variation of the estimates. They also allow the activity of one neuron to be informative about impending perceptual decisions or motor actions on single trials. In extrastriate visual area MT of the rhesus macaque, for example, some but not all neurons show nonzero "choice probabilities" for perceptual decisions or non-zero "MT–pursuit" correlations between the trial-by-trial variations in neural activity and smooth pursuit eye movements. To understand the functional implications of zero versus nonzero correlations between neural responses and impending perceptions or actions, we took advantage of prior observations that specific frequencies of local field potentials reflect the correlated activity of neurons. We found that the strength of the spike-field coherence of a neuron in the gamma-band frequency range is related to the size of its MT–pursuit correlations for eye direction, as well as to the size of the neuron–neuron correlations. Spike-field coherence predicts MT–pursuit correlations better for direction than for speed, perhaps because the topographic organization of direction preference in MT is more amenable to creating meaningful local field potentials. We suggest that the relationship between spiking and local-field potentials is stronger for neurons that have larger correlations with their neighbors; larger neuron–neuron correlations create stronger MT–pursuit correlations. Neurons that lack strong correlations with their neighbors also have weaker correlations with pursuit behavior, but still could drive pursuit strongly.

Introduction

The nature of the brain's population decoding computation has been the topic of many studies, not only for sensory-motor transformations, but also for perceptual decisions. For both functions, correlated variation in the sensory population response is an important factor in determining the variation of the behavioral output (Zohary et al., 1994; Britten et al., 1996; Shadlen et al., 1996; Medina and Lisberger, 2007; Schoppik et al., 2008; Huang and Lisberger, 2009; Haefner et al., 2013). Further, correlated variation allows the discharge of single sensory neurons to be informative about impending perceptual decisions (Britten et al., 1996) or motor actions (Hohl et al., 2013). Because local field potentials (LFPs) provide a window into correlated variation across a neural population, we have asked whether LFPs reveal the mechanisms behind the trial-by-trial correlations between responses of single neurons and behavior.

The LFP is a consequence of the collective electrical potentials from synchronized synaptic currents and/or spiking activity in the vicinity of a recording electrode (Mitzdorf, 1985; Katzner et al., 2009; Berens et al., 2012). Recent studies have focused on the possible functional importance of specific frequency bands of LFP for higher cognitive functions and/or basic sensory processing (Fries et al., 2001; Pesaran et al., 2002; Womelsdorf et al., 2006; Gregoriou et al., 2009; Bosman et al., 2012; Ray et al., 2013). In the present study, however, our goal was to use the LFP to understand why some, but not all, middle temporal area (MT) neurons show a trial-by-trial "neuron–behavior" correlation with the initiation of the smooth pursuit eye movements for a moving target (Hohl et al., 2013). Does the absence of neuron–behavior correlation mean that a given neuron does not contribute to the behavior?

A prior analysis showed that the strength of neuron–behavior correlations depends on many factors (Schoppik et al., 2008); the relative contribution of those factors is telling for the organization of the neural sensory-motor system. Larger trial-by-trial correlations between the spike counts of neurons in the population, stronger connections to downstream circuits, and lower amounts of noise added downstream to a given site all promote larger values of neuron–behavior correlations. Thus, there are multiple explanations for the observation that some MT neurons have strong MT–pursuit correlations while others have none (Hohl et

Received Aug. 13, 2013; revised Oct. 8, 2013; accepted Nov. 7, 2013.

Author contributions: J.L. and S.G.L. designed research; J.L. performed research; J.L. analyzed data; J.L. and S.G.L. wrote the paper.

This research was supported by the Howard Hughes Medical Institute and National Institutes of Health Grant EY03878. We thank John H. R. Maunsell and members of the Lisberger Laboratory for helpful comments on an earlier version of the manuscript. We thank K. MacLeod, E. Montgomery, S. Tokiyama, S. Ruffner, D. Kleinhesselink, D. Wolfgang-Kimball, D. Floyd, S. Happel, and K. McGary for technical assistance.

The authors declare no competing financial interests.

Correspondence should be addressed to Joonyeol Lee, Department of Neurobiology, Duke University, 412 Research Drive, Durham, NC 27710-0001. E-mail: joonyeol@neuro.duke.edu.

DOI:10.1523/JNEUROSCI.3478-13.2013

 0270-6474/13/3319677-12$15.00/0

al., 2013). The wide range of MT–pursuit correlations could result from variation in how well a given MT neuron is correlated with its neighbors, heterogeneity in the amount of noise added downstream for different neurons, or variation in the strength of connections to the motor pathways.

If specific frequency bands of LFP indeed reflect the degree of correlated activity between neurons (Womelsdorf et al., 2012; Jia et al., 2013), then the properties of the LFP might reveal how strongly a given neuron correlates with its neighbors, and might predict its MT–pursuit correlation. Indeed, we find that spike-field coherence in the gamma-band frequency is a good predictor for the size of MT–pursuit correlation, and for the neuron–neuron correlation between pairs of neurons. Thus, MT–pursuit correlations are an index of the correlations of a neuron with its neighbors, but might be zero even if a neuron has strong downstream connections to the motor circuits. The same conclusion would apply to the choice probabilities for perceptual decisions (Britten et al., 1996).

Materials and Methods

Two adult male rhesus monkeys were trained to perform a smooth pursuit eye movement task in exchange for juice that was provided as a reward for the correct behavior. Before training, we had performed two separate surgeries. A head holder was implanted on the skull for head restraint, and a scleral search coil was implanted in one eye (Ramachandran and Lisberger, 2005) using aseptic surgical procedures. After finishing behavioral training, we implanted a stainless steel chamber on the skull for a vertical approach to the MT in the extrastriate visual cortex. All experiments were conducted at University of California, San Francisco (UCSF) using methods that had been approved in advance by the Institutional Animal Care and Use Committee at UCSF. Methods conformed to the National Institutes of Health *Guide for the Care and Use of Laboratory Animals.*

Data acquisition

Visual stimuli were displayed on an analog oscilloscope (1304A, HP) that provided 2^{16} steps along each axis and temporal resolution of 500 Hz. The oscilloscope was driven by the outputs of 16-bit digital-to-analog converters on a digital signal-processing board embedded in the computer that controlled the experiments. The scope was placed 260 mm from the monkey and the screen covered 55° by 44° of the horizontal and vertical visual field. During experiments, we sampled horizontal and vertical eye position and eye velocity at 1 kHz on each channel. Voltages proportional to eye velocity were obtained by running the eye position voltages from the eye coil electronics through an analog circuit that differentiated signals at frequencies $<$25 Hz and filtered signals at higher frequencies ($-$20 dB per decade).

We lowered two to five quartz-insulated tungsten electrodes with impedances from 2 to 4 MΩ (at 1 kHz) into area MT to record spikes and LFPs using the Mini-Matrix System (Thomas Recording GmbH). The electrical signals from each electrode were filtered in parallel to separate LFPs and spikes. Signals were low-pass filtered with a cutoff frequency of 170 Hz and digitized at a sampling rate of 2 kHz for LFPs; signals were high-pass filtered with a cutoff frequency of 150 Hz and digitized at a sampling rate of 40 kHz for action potentials using the Plexon MAP.

To identify the responses characteristics of neurons during experiments, we discriminated single-unit spikes on-line using a window discriminator. For detailed data analysis, we sorted spikes off-line (Plexon). We used a principal component analysis for the initial sorting and then pruned the sorted signals by inspecting individual waveforms visually. We paid special care to the isolation of spikes from single neurons, and we included neurons for further analysis only when they formed distinct clusters in principal component analysis space. Sorted spikes were converted to time stamps with a time resolution of 1 ms and were inspected again visually to look for obvious sorting errors.

Experimental design

We ran three types of experiments that were used for the following different purposes: image motion during fixation; target motion leading to pursuit; and target motion leading to pursuit with image stabilization. We used the data obtained during image motion with fixation to quantify the receptive field properties of each neuron and also to analyze the spike-field coherence for image motion without pursuit. We used the data obtained during the two pursuit experiments to analyze the spike-field coherence, while animals generated visually guided pursuit eye movements under conditions with and without the possibility that their own eye movements could modify the image motion across the retina.

We began each day's experiment by lowering electrodes into MT and isolating neurons on as many electrodes as possible. Frequently, we obtained only a single good site, but on 39 experiments we recorded from two or more well isolated neurons simultaneously. After we were satisfied with the location of the electrodes, we performed a number of tests to characterize receptive field properties of isolated MT neurons while the monkey fixated a stationary spot. We identified the approximate receptive field location, and the preferred direction, speed, and size of a given MT neuron with hand-controlled visual stimuli.

In the first experiment for each neuron, we quantified the direction tuning, speed tuning, size tuning, and orientation tuning of the cell with stimulus motion during fixation of a stationary spot. A square patch of random dots with 100% coherence served as the visual stimulus. Every dot in the patch moved coherently with infinite lifetime; dot density was 2 dots/deg^2. Stimuli were presented in behavioral trials that began with 600 to 1000 ms of fixation and then included four to eight different motion stimuli of 256 ms duration with interposed stationary epochs of 300 ms duration. We presented stimulus motion in 12 directions near the preferred speed for direction tuning, at 7 speeds near the preferred direction for speed tuning, and random dot patches of 5 sizes moving near the preferred speed and direction for size tuning. We computed tuning curves on-line during the experiment using Gaussian or circular Gaussian functions for direction tuning and a log Gaussian function for speed tuning. We then used the tuning curves to determine stimulus parameters for the main data collection from each neuron. For recordings from one neuron, we used a stimulus that was as close as possible to the preferred stimulus for the neuron. For recordings from pairs of neurons, we chose a stimulus that was a compromise between the preferred responses of the two neurons. If the preferences of the two neurons were too different to find a good compromise, we discarded the pair from further analysis. In both cases, we also were constrained by the need to choose a stimulus direction that would evoke good presaccadic pursuit. This limited us to combinations of preferred direction and receptive field location so that the stimulus would not take the target directly away from the position of fixation. We excluded neurons from further analysis if the tuning curves explained $<$50% of the variance in the speed or direction tuning data.

In the second experiment, we recorded spike activity and the associated LFPs during many repetitions of the initiation of smooth pursuit eye movements for one or a few target motions. Target motions were presented in individual trials, where each trial started with a fixation point in the center of the screen. After the monkey fixated on the target for 300 ms, a static patch of random dots (typically 4–8°^{2}) appeared in the receptive field of the cell, and remained on and stationary for a random duration of 500 to 1300 ms (Fig. 1) while the monkey fixated within 1° of the stationary target. Then, the patch underwent local motion within a stationary, invisible aperture for 192 ms (monkey N) or 126 ms (monkey R) with parameters that were optimized for the size, direction, and speed preferences of the neuron under study. Sometimes, we had to find a compromise between suboptimal parameters for the neuron under study and target motion parameters that caused better initiation of pursuit eye movements, while remaining within the range of parameters that evoked good responses in the neuron. After the period of local motion, the dots and invisible aperture moved together for a random duration of 500 to 700 ms. The monkey received a reward if he tracked the motion stimulus within the bounds of stimulus size until the end of the trial. We also presented pursuit stimuli of the same speed and size, but with motion in the opposite direction from the optimal stimulus to balance the pursuit

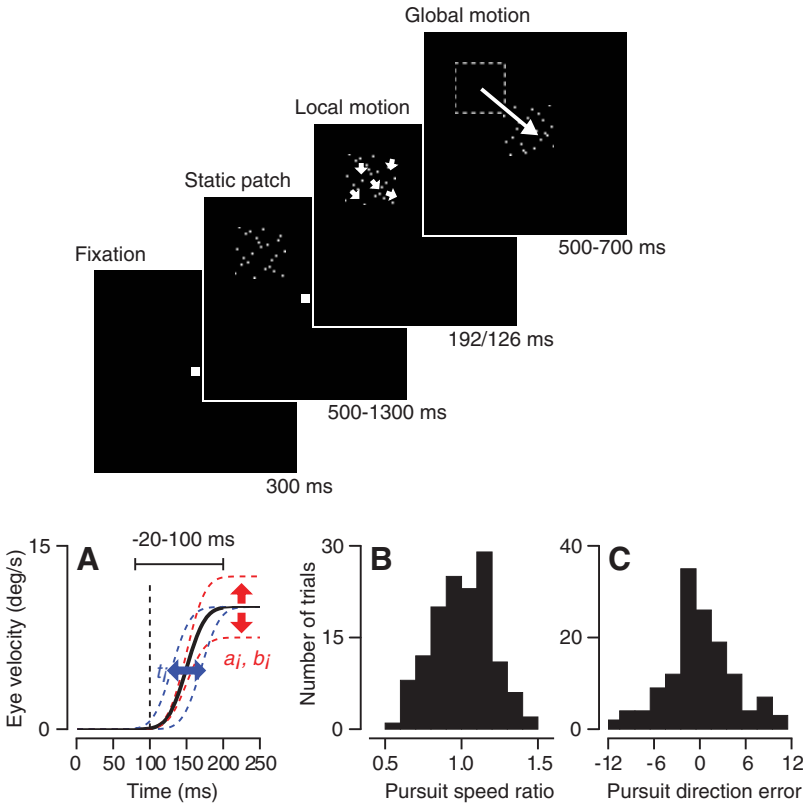

Figure 1. Temporal structure of sensory-guided smooth pursuit eye movement task and estimation of pursuit variation. Top, The sequence of stimulus presentation and motion in a typical pursuit trial. ***A***, An illustration to show the procedure used to describe pursuit variation in terms of three components: direction, speed, and latency. Vertical dashed line is the time of initiation of pursuit. ***B***, ***C***, Distributions of the estimates of the speed and direction components for an example session.

conditions and prevent the animal from anticipating the target motion correctly. We analyzed only data for motion near the preferred direction.

In a third experiment, conducted on a subset of neurons, we stabilized the moving stimulus on the retina from 400 ms before to 126 ms after the onset of stimulus motion, while expecting the monkey to initiate smooth pursuit eye movements. We intermixed trials with and without stabilization in random order, so the monkey could not anticipate correctly whether the current trial would use image stabilization. To stabilize the stimulus on the retina, the computer monitored eye position and adjusted the position of the visual stimulus with a temporal resolution of 500 Hz and spatial resolution of 0.04°. We minimized potential artifacts from the temporal delay of visual motion by using an analog display oscilloscope with a temporal resolution of 2 ms (500 Hz), which is beyond the fastest temporal sensitivity of MT neurons (Bair and Koch, 1996; Buracas et al., 1998). We used the method of Morris and Lisberger (1987) to test whether calibration of eye position was good enough to consider vision "stabilized."

To increase the variation in the initiation of pursuit, the local motion within a stationary aperture used a pattern of noisy dots that comprised "random walk motion" (Osborne and Lisberger, 2009). Each stimulus was defined by a base direction of motion. The motion of each dot was in a direction selected randomly from a uniform distribution that was bounded by ±60° relative to the base direction. The direction of motion changed every 12 ms for each dot. The resulting visual stimulus appeared "noisy," but evoked pursuit initiation of high quality. We used the same random number seed for every stimulus in a day's experiment, so that every presentation of the pursuit target comprised exactly the same, noisy, visual motion stimulus.

After the experiment, we screened all trials visually and excluded from further analysis any pursuit trials that contained saccades or microsaccades between 200 ms (monkey N) or 400 ms (monkey R) before target motion onset and 230 ms after target motion onset. We also excluded any fixation trials that contained microsaccades in the interval from 50 ms before to 300 ms after motion onset. We defined a change in eye position as a microsaccade if its peak speed exceeded 10°/s. The results were the same when we repeated the analysis without excluding epochs with microsaccades.

Decomposition of pursuit eye movements

Osborne et al. (2005) showed that ~90% of the variation in the initiation of pursuit eye movements can be explained by three dominant principal components, and the components can be expressed in terms of errors in estimating target speed, target direction, and the time of target motion onset. We have performed a similar decomposition of the initiation of pursuit, but we took a more direct approach because the method of Osborne et al. (2005) requires many more stimulus conditions than are feasible for a single-neuron recording experiment.

First, we averaged the horizontal and vertical components of eye velocity across all repetitions of a given stimulus condition. We estimated the mean pursuit latency by visual inspections of the average traces. We measured the average eye velocity at the end of the open-loop period (interval from 200 to 220 ms after target motion onset), determined the average pursuit direction in polar coordinates, and rotated all pursuit traces so that pursuit direction at the end of open-loop period averages 45°. Rotation does not change the data, but simplifies the math for estimation of direction and speed variation. For each trial i, we then assigned two scaling factors, a_i and b_i, and a latency, t_i, by shifting and scaling the mean horizontal and vertical traces (H_{template} and V_{template}) from 20 ms before to 100 ms after the mean latency to match the mean (Fig. 1*A*), as follows:

$$\hat{H}_i(t_i) = H_{\text{template}} \times a_i \quad (1)$$

$$\hat{V}_i(t_i) = V_{\text{template}} \times b_i. \quad (2)$$

We estimated a_i, b_i, and t_i by minimizing the sum of squared errors (NOMAD algorithm; Le Digabel, 2011). At this point, we excluded 11% of trials because the optimization procedure accounted for <90% of the within-trial variance in horizontal and vertical eye velocity.

From the estimates of a_i, b_i, and t_i, we derived the deviation from the mean, or "residuals" for eye speed, direction, and timing for each pursuit trial as follows:

$$\Delta S_i = \sqrt{(H_{\text{template}} \times a_i)^2 + (V_{\text{template}} \times b_i)^2} \quad (3)$$

$$\Delta\theta_i = \tan^{-1}\frac{V_{\text{template}} \times b_i}{H_{\text{template}} \times a_i} \quad (4)$$

$$\Delta t_i = t_i. \quad (5)$$

Strictly speaking, the residuals on the left side of Equations 3 and 4 are time-varying functions. However, rotation of the data to a mean direction of 45° guarantees that $H_{\text{template}} \approx V_{\text{template}}$, so that Equations 3 and 4 reduce to the following:

$$\Delta S_i \approx (\sqrt{a_i^2 + b_i^2}) \times \text{constant}. \quad (6)$$

$$\Delta\theta_i \approx \tan^{-1}\frac{b_i}{a_i}. \quad (7)$$

The decomposition into Δs_i, $\Delta\theta_i$, and Δt_i explained ~87.5% of the trial-over-trial variation in the initiation of pursuit eye movements, consistent with a previous study that used a slightly different principal component analysis (Osborne et al., 2005). Figure 1, *B* and *C*, shows distributions of estimated Δs and $\Delta\theta$ from an example experimental session. Consistent with the previous study (Osborne et al., 2005), both estimates follow normal distributions.

Neural data analysis

In the foregoing descriptions of analysis procedures, we mentioned the time windows we used for each analysis. The justification for the choice of analysis windows appears in a separate section at the end of the Materials and Methods.

We computed trial-by-trial correlations between neural responses and the direction or speed residuals using Spearman's correlation analysis. We counted spikes in a window from 20 to 100 ms after the mean response latency of each neuron. To ensure that we were analyzing spikes that contributed to the first 100 ms of pursuit, we included only neurons with response latencies of <80 ms. We excluded outlier trials with pursuit residuals of >3 SDs and with spike counts that were >5 SDs from the mean. As a result of excluding outliers, ~3% of trials were excluded from further analysis. We conducted analysis on neurons that provided >100 repetitions of the relevant target motions. After all data editing and exclusions, we performed quantitative analysis on 96 of the 144 neurons we recorded.

Because the initiation of pursuit overlaps with the spike count window, we were concerned about a possibility that pursuit eye movement could affect the spike count used in the correlation, even though it is unlikely given the response latency of each neuron. Also, eye movements of fixation before motion onset might affect pursuit behavior and spiking activity (Hohl and Lisberger, 2011). We controlled for these factors by using a partial correlation with fixation or initial pursuit eye movements that occurred before the spike count window as a control variable. We performed the analysis for eye movements in 60 ms windows that were centered 60, 30, and 0 ms before the spike count window for a given cell, and we present data for partial correlations using the window that had the largest impact on the MT–pursuit correlations. In fact, our conclusions did not depend on whether or not we used partial correlation.

We used a fixed time window from 40 to 160 ms after the onset of target motion to perform correlations between the spike counts in pairs of neurons. As outlined above, we used partial correlation for the neuron–neuron correlation analysis, with the eye movements before the analysis interval as a control variable. We included pairs of neurons in our sample only when the number of repetitions of target motion was >100 and the mean response latencies for both neurons in the pair were <100 ms. These criteria resulted in analysis of 39 of 54 pairs.

We preprocessed the LFP data with a Butterworth filter to remove 60 Hz line noise. The filter used pass-bands of 59 and 61 Hz and stop-bands of 56 and 64 Hz, and at least 35 dB of attenuation at the stop-band. We then analyzed the "spike-field coherence" between the spikes of single neurons and the LFP recorded from the same electrode using Chronux MATLAB toolbox (Bokil et al., 2010). For frequency ranges between 20 and 170 Hz, we estimated spike-field coherence using a fast Fourier transform after multitapering (Mitra and Pesaran, 1999) with three tapers for pursuit experiments and with five tapers for fixation experiments. The tapering strategy resulted in a spectral smoothing of ±20 Hz for all data because the spectral analysis used 100 ms of data for the pursuit experiments, and 150 ms of data for the fixation experiments. We performed a separate analysis for the lower frequencies (1–20 Hz) using a Hanning window as a taper. For both frequency ranges in both pursuit and fixation experiments, we calculated spike-field coherence in 100 or 150 ms sliding windows with a step size of 10 ms.

The coherence in each epoch is defined by the following:

$$C(f) = \frac{S_{\text{spike,LFP}}(f)}{\sqrt{S_{\text{spike,spike}}(f)\, S_{\text{LFP,LFP}}(f)}}, \tag{8}$$

where $S(f)$ is the spectrum for the simultaneously recorded spike and LFP. Because the number of trials affects the coherence estimate, we transformed the coherence using the variance stabilization method (Bokil et al., 2007). The transformed coherence is given by the following:

$$\acute{C}(f) = \tanh^{-1}(c(f)) - \frac{1}{\nu_0 - 2}, \tag{9}$$

where degrees of freedom, ν_0, equals twice the number of tapers multiplied by the number of trials.

We calculated the power of the LFP during the first 150 ms after the onset of stimulus motion, using the data from the prior 150 ms as a baseline. For analysis of spike-field coherence, we focused on the first 100 ms of spiking activity for reasons enunciated in the last section of Materials and Methods. During the interval we have used, both the spiking and the LFP can display transient responses, creating a potential confound that might cause our estimates of spike-field coherence to be inaccurate at low frequencies (Jarvis and Mitra, 2001). To mitigate this confound, we shuffled the spike train and LFP recordings across trials to obtain 1000 estimates of spike-field coherence that would include any confound from transients in the signals without any legitimate spike-field coherence. The "null distributions" from the shuffle analysis allowed us to obtain a *z*-score as a function of frequency in the analysis of spike-field coherence for each neuron, as follows:

$$z(f) = \frac{\acute{C}_{\text{original}}(f) - E[\acute{C}_{\text{shuffled}}(f)]}{\sigma[\acute{C}_{\text{shuffled}}(f)]}, \tag{10}$$

where $\acute{C}(f)$ represents the variance-stabilized spike-field coherence at frequency *f*, and $E(x)$ is the mean of *x*. To control for any effect of the remnants of spikes in the LFP, we removed the potentials from the interval between −1 and 2 ms from the time of spiking and interpolated linearly between the potentials at the ends of the interval. Excision of the data surrounding spikes from the LFP did not alter our results materially, and we have chosen to show the analysis from data without excisions.

We computed spike-triggered averages of the LFP after filtering the LFP using Butterworth digital bandpass filters with pass bands of 10–30, 30–80, or 80–170 Hz. Maximum attenuations in the stop bands were adjusted individually to minimize artifacts and maximize accuracy. We segmented the filtered LFPs into time windows of ±64 ms relative to the time of each spike, and averaged the bandpass-filtered LFPs across all spikes for a given neuron, using spikes that occurred between 40 and 140 ms after the onset of stimulus motion. The results were noisier, but otherwise indistinguishable when we used spikes from 20 to 100 ms after the onset of neuronal responses, as we had for the MT–pursuit correlation analysis.

To test the null hypothesis and control for LFPs that were driven by common inputs due to the sensory stimulus, we shuffled the spike trains relative to the LFPs 500 times and calculated the shuffle predictor for the spike-triggered average of the LFP. To obtain the spike-triggered averages presented in the Results, we subtracted the shuffled spike-triggered average from the direct spike-triggered average obtained with the original data. Finally, we discarded phase information from the spike-triggered averages to pool them for the population analysis by shifting them in time to align the nearest peak or trough with the time of the spikes, and then inverting the average if necessary so that the spike would be aligned with a trough.

Rationale for choice of analysis windows

The analysis windows for neural data differed for different data analyses. The choices we made were not arbitrary, but rather were intended to use appropriate windows in the face of competing constraints. The analysis windows we used are summarized in Table 1, and we explain the choices we made in this section.

The end of the analysis interval almost always was driven by the need to avoid including data that might be influenced by feedback from pursuit eye movements, which would alter image motion as well as LFPs and MT neural responses. Given that the average pursuit onset latency is ~100 ms and the latency of MT responses is >40–60 ms, a time window that ends within 160 ms of the onset of target motion excludes feedback effects of pursuit initiation on the responses of MT neurons or the LFPs.

Table 1. Analysis windows for different forms of data analysis

Condition	Time window
Spike count for MT–pursuit correlation	20–100 ms after neuronal response onset
Spike count for neuron–neuron correlation	40–160 after stimulus motion onset
Spike-field coherence and spike-triggered averages for pursuit direction	40–140 ms after stimulus motion onset
Spike-field coherence for pursuit speed	20–120 ms after stimulus motion onset
Spike-field coherence for neuron–neuron correlation	40–140 ms after stimulus motion onset
Spike-field coherence for fixation	140–290 ms after stimulus motion onset
Spike-triggered average of LFP	40–140 ms after stimulus motion onset
LFP power analysis for spontaneous activity	150 ms before stimulus motion onset
LFP power analysis for visual response	150 ms after stimulus motion onset

Spike counts. We chose the interval from 20 to 100 ms after the onset of the neural response for MT–pursuit correlations to ensure that we captured the spikes that would drive the initial part of the pursuit response, while terminating the analysis window early enough to avoid any effects of pursuit initiation on MT responses. To analyze neuron–neuron correlations, we used a wider analysis window from 40 to 160 ms after the onset of stimulus motion to allow us to perform meaningful analysis for pairs of neurons that had quite different response latencies, while still comparing responses over the same time intervals in the two neurons.

Spike-field coherence. We used an interval from 40 to 140 ms after the onset of target motion for the analysis of spike-field coherence for pursuit direction as a compromise between the increased resolution provided by a longer interval and the need to include only spikes that occurred before pursuit initiation could affect MT responses through feedback. We used a slightly earlier interval, from 20 to 120 ms after the onset of stimulus motion, for pursuit speed because this was the only interval that showed a statistically significant effect of spike-field coherence on MT–pursuit correlations for speed. We used a window from 40 to 140 ms after the onset of target motion for studying the relationship between spike-field coherence and neuron–neuron correlations, again as a compromise to allow us to include pairs of neurons with quite different response latencies while preventing contamination of the spikes or LFPs through feedback from the initiation of pursuit. We used a delayed time window from 140 to 290 ms after the onset of stimulus motion for the analysis of spike-field coherence for stimulus motion during fixation because (1) the absence of pursuit obviated concerns about feedback altering MT responses, and (2) it allowed us to cleanly avoid the early transient responses that could bring artifacts.

Spike-triggered averages. We used the window from 40 to 140 ms after the onset of target motion to include 25% more spikes in the analysis relative to the 80 ms duration window used for MT–pursuit correlations.

LFP power analyses. We used windows with durations of 150 ms to improve the frequency resolution of the results.

Results

We measured LFPs and the spiking activity of single neurons simultaneously in area MT of two rhesus monkeys during pursuit tracking of moving visual stimuli. During the initiation of pursuit, we measured the trial-by-trial correlation between the variation in the spike counts of MT neurons, and the variation in the direction and speed of the initiation of pursuit behavior. We also measured the coherence between the spiking activity of each neuron and the LFP recorded from the same electrode. We found that large spike-field coherence in the frequency range of gamma oscillations (>30 Hz) predicts large values of MT–pursuit correlation for the direction of eye motion, as well as strong trial-by-trial correlations between the spike counts in pairs of neurons that were recorded simultaneously. We conclude that MT neurons are strongly correlated with pursuit behavior if (and only if) they also are strongly correlated with neurons that prefer similar stimulus motions.

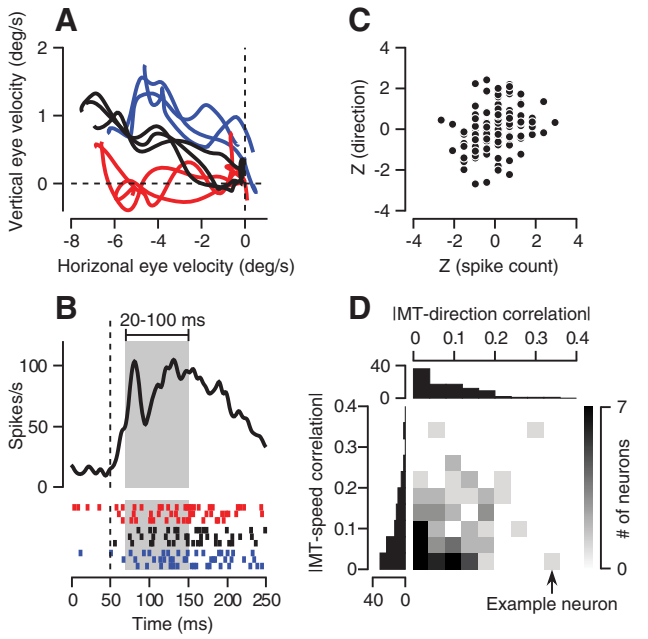

Figure 2. Example data for pursuit direction and neural responses, and the population distribution of MT–pursuit correlations. ***A***, Example eye velocity traces plotted in polar coordinates. ***B***, The peristimulus time histogram of an example neuron and a raster plot for nine individual trials. The gray-shaded area marks the analysis interval for spike counts. Vertical dashed line shows the onset of neuronal responses. The colors of the raster lines match with the eye movements in ***A***. ***C***, Scatter plot for MT–pursuit direction correlations. Each symbol represents data from a different trial (Spearman's $R = 0.33$). ***D***, Joint distribution of MT–pursuit correlations for speed and direction. The arrow marks the example neuron used in the other panels.

MT–pursuit correlations

Figure 2*A* illustrates that different individual pursuit responses started in different directions, and Figure 2*B* shows the trial-by-trial variation in the spike trains associated with the different directions of pursuit. It is not easy to infer a correlation, however, from a few example trials. Instead, quantitative analysis of an average of 153 trials for each single neuron revealed correlations between eye direction and spike count (Fig. 2*C*). To perform the analysis, we decomposed the variation in pursuit initiation from each trial into three components related to variation in eye direction, speed, and latency using an approach described in Materials and Methods and Figure 1*A*. The scale factor for speed, rotation for direction, and time shift for latency characterized the behavior in each individual trial by a trio of values that estimate its variation from the mean. We then computed the trial-by-trial correlation in the variation of the three parameters used to describe the initiation of pursuit and the spike count of each MT neuron.

In our sample (Fig. 2*D*), some neurons showed high MT–pursuit correlations between spike count and the direction of pursuit eye movements, but others show almost no correlation with the direction of pursuit. The same range of MT–pursuit correlations appeared for the speed of pursuit eye movements, in agreement with the results of Hohl et al. (2013) using a different sample of MT neurons. The distribution of MT–pursuit correlations was biased toward zero for both target direction and speed, and there was no correlation between the sizes of MT–pursuit correlation for the two components of eye movement (Spearman's $R = 0.16$, $p > 0.1$).

All prior reports have found impressive variation across neurons in how informative the trial-to-trial variation in spiking is

about the variation in perceptual decisions (Britten et al., 1996; Nienborg and Cumming, 2006; Palmer et al., 2007) or motor actions (Krauzlis, 2003; Snyder et al., 2006; Schoppik et al., 2008; Hohl et al., 2013). Our premise is that the same mechanisms are operating for both perceptions and actions, and our goal in the rest of the article is to understand those mechanisms through exploration of the neuron-to-neuron variation in the strength of MT–pursuit correlations.

Spike-field coherence predicts MT–pursuit correlation for eye direction

Spike-field coherence captures the phase relationship between the LFP and spikes. If spikes occur selectively at a certain phase of a given frequency of the LFP, then the spike-field coherence at that frequency will be one. If the phase relationship is random, then the spike-field coherence will be zero. Before presenting the results of spectral analysis, we show the intuitive basis for spike-field coherence by calculating spike-triggered averages of the LFP. To perform this analysis, we filtered the LFPs using different frequency bands, yielding the three continuous traces in Figure 3*A*.

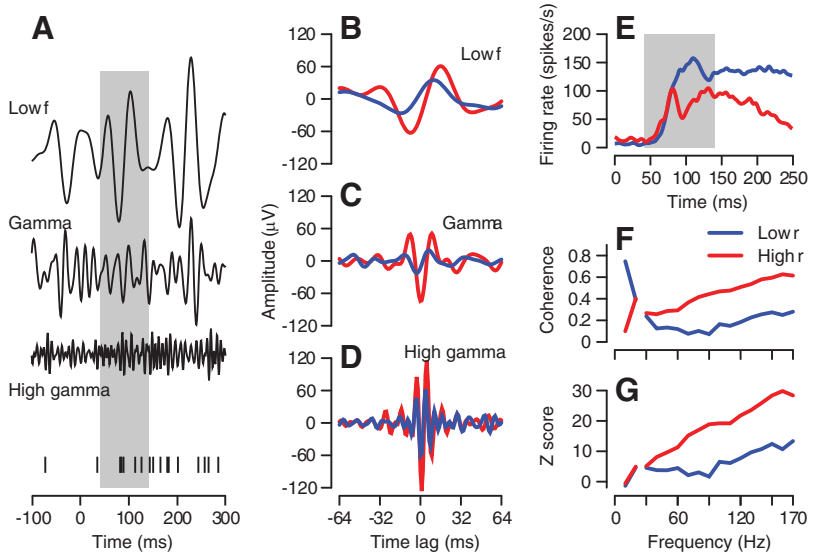

Figure 3. Spike-triggered averages of local field potential and spike-field coherence for two representative neurons. ***A***, Bandpass-filtered LFPs and spike train from an example trial. Gray-shaded area shows the interval used for data analysis. ***B–D***, Spike-triggered averages of LFPs for low-frequency band (10–20 Hz), gamma frequency band (30–80 Hz), and high-gamma frequency band (80–170 Hz). ***E***, Peristimulus time histograms. ***F***, Spike-field coherence. ***G***, Shuffle-corrected *z*-scores of spike-field coherences. In ***B–G***, the red and blue traces show data for two neurons with high ($R = 0.33$) versus low ($R = 0.03$) MT–pursuit correlations for pursuit direction.

The spike-triggered averages of two example neurons with large versus small MT–pursuit correlations suggest that some features of the LFP may be correlated with the magnitude of the MT–pursuit correlation. After bandpass filtering to include frequencies from 30 to 80 Hz (gamma band), the spike-triggered average of LFPs for the neuron with a larger MT–pursuit correlation (Fig. 3*C*, red trace) showed a strong peak in the spike-triggered average. The neuron with a smaller MT–pursuit correlation showed smaller spike-triggered averages of LFPs (blue trace). The difference was strongest in the gamma frequency band, but also was present in the spike-triggered averages computed after bandpass filtering to include frequencies from 10 to 30 Hz or from 80 to 170 Hz (Fig. 3*B*,*D*).

The difference among neurons in the relationship between spikes and the LFPs persisted and was documented more fully when we analyzed spike-field coherence using the multitapering method described in Materials and Methods. For the two neurons we have chosen for illustration, a spike had larger coherence with LFPs in the high-frequency band, especially the gamma band, for the neuron that had a bigger MT–pursuit correlation for direction in the initiation of pursuit (Fig. 3*F*, red vs blue traces). The difference persisted and became cleaner (Fig. 3*G*) when we eliminated the artifacts from transient responses at the onset of target motion by generating *z*-scores relative to the distribution obtained by a shuffle analysis (see Materials and Methods).

The relationship between spike-field coherence and MT–pursuit correlation for direction was clear across all 96 MT neurons that provided enough data for analysis (monkey R, $n = 53$; monkey N, $n = 43$). We sorted the neurons in our sample by the size of the MT–pursuit direction correlation, and chose the two groups of 20 neurons that had largest (mean $|R| = 0.18$) and smallest (mean $|R| = 0.02$) MT–pursuit direction correlations. The firing rate responses to motion were very similar in the two groups (Fig. 4*A*), the LFPs of the two groups had the same power (Fig. 4*G*), and the groups did not differ in the number of neurons they included from each monkey (monkey R, $n = 11$ for each group; monkey N, $n = 9$ for each group).

The two groups of neurons differed markedly in the spike-triggered average of LFPs for the gamma band and the high gamma band (Fig. 4*B*,*C*), but less so in the low-frequency band (Fig. 4*D*). In the gamma band, many points in the average traces showed statistically significant differences near the time of spiking (two-tailed Wilcoxon rank sum test, $p < 0.01$). The two groups showed statistically significant differences (one-tailed Wilcoxon rank sum test: $p < 0.05$, gray bars; $p < 0.01$, green bars) in the raw spike-field coherence (Fig. 4*E*) and in bias-corrected *z*-scores (Fig. 4*F*) in the gamma band and some of the high-gamma-band frequencies. The similarity of the LFP power spectrum amplitudes for the two groups of neurons (Fig. 4*G*) argues that differences in the spike-triggered average and the spike-field coherence must reflect differences in the phase relationship between the LFP and the spikes, and not simply differences in the amplitudes of the LFPs.

The properties of the visual stimulus are not a likely cause of the differences between the two groups of neurons, because the properties did not vary systematically between groups. The deviation of target motion direction from the preferred direction of each neuron was 15.0 ± 3.7° versus 12.9 ± 2.5° in the high- versus low-correlation groups ($p > 0.9$, Wilcoxon rank sum test). The deviation of target speed from the preferred speed of each neuron in $\log_2$ units did not differ between groups ($p > 0.3$). The absolute sizes of the pursuit target were 6.5 ± 0.4°^{2} versus 5.9 ± 0.3°^{2} in the high- versus low-correlation groups ($p > 0.19$). The difference between preferred stimulus size of each neuron and target size were 3.4 ± 0.5°^{2} versus 4.3 ± 1.3°^{2} in the high- versus low-correlation groups ($p > 0.65$). All errors are given as SEMs.

To summarize the relationship between spike-field coherence and MT–pursuit correlations for eye direction, we computed the correlation coefficient across neurons between the *z*-scores for

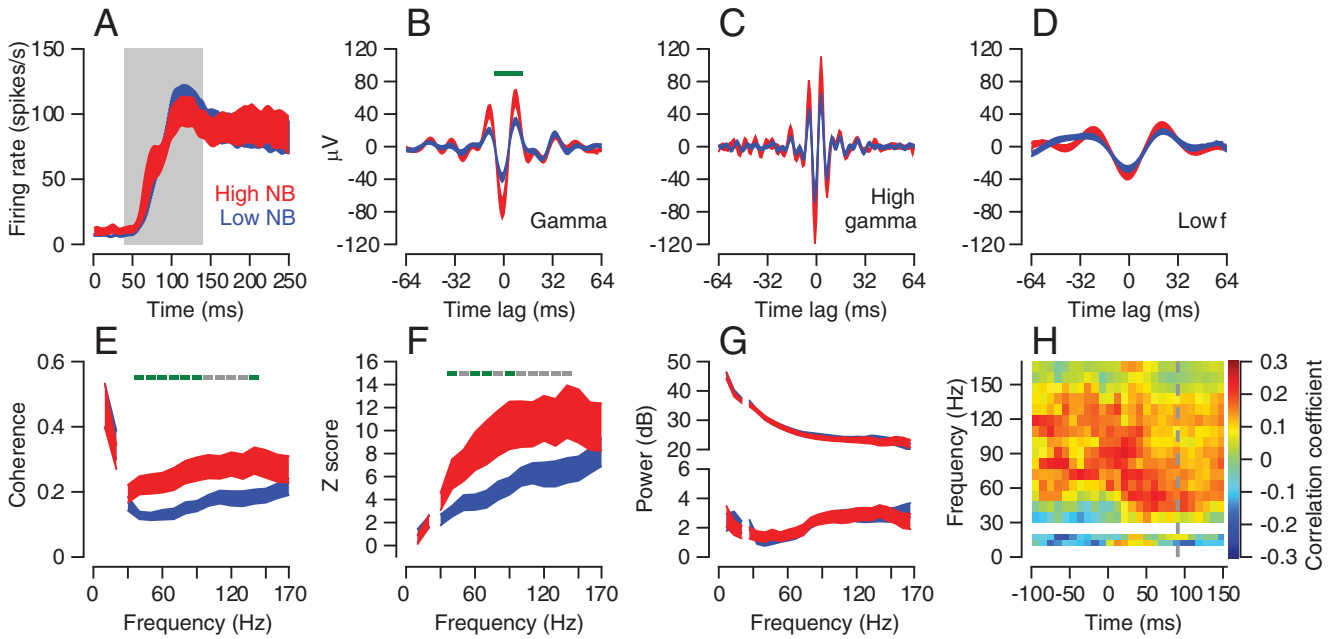

Figure 4. Relationship between LFPs and MT–pursuit correlation for direction. Red and blue ribbons show mean ± 1 SE for groups of 20 neurons with the highest and lowest amplitude MT–pursuit correlations. ***A***, Population average peristimulus time histograms during pursuit initiation. Gray-shaded area represents the time interval used for the group comparison. ***B–D***, Spike-triggered average LFPs of the two groups for gamma-band frequency, high-gamma-band frequency, and low frequencies. ***E***, Spike-field coherences for the two groups. ***F***, Shuffle-corrected *z*-scores of the two groups. In ***B***, ***E***, and ***F***, the green and gray bars at the top of the graph show time points where the two groups are significantly different at $p < 0.01$ or $p < 0.05$ (two-tailed Wilcoxon rank sum test for ***B***, one-tailed test for ***E*** and ***F***). ***G***, Top and bottom graphs, Raw power spectrum and corrected power spectrum: spectrum during visual motion minus spectrum during fixation. ***H***, Correlation across all of the 96 neurons for the relationship between shuffle-corrected *z*-scores and MT–pursuit direction correlations. The color of each pixel shows Spearman's *R* for a given time point and frequency. Gray dashed line shows the epoch where the group comparisons were performed.

the spike-field coherence analysis and the size of the MT–pursuit direction correlation. In Figure 4*H*, the color of each pixel indicates the value of the correlation at a given time during the LFP and at the frequency indicated by the position of the pixel on the *x*- and *y*-axes. Consistent with the impression given by comparison of the two extreme groups of neurons, the values of the MT–pursuit correlations were most strongly related to the spike-field coherence in the gamma-band frequencies, and less strongly in the low-frequency band and high gamma frequency band (>120 Hz). The same pattern appears over most of the analysis time window, although the strength of the correlations tends to decrease starting for the LFPs recorded at about the time of pursuit initiation, ~100 ms after the onset of target motion. The stronger predictive power of spike-field coherence in the gamma band, and the weaker predictive ability in the high gamma band is important because it argues against bleed-through from spikes to LFPs as a cause of the relationship between spike-field coherence and MT–pursuit correlation. Bleed-through should have the largest effect in the high gamma band (Ray and Maunsell, 2011).

Figure 4*H* shows that the correlation between the *z*-scores and the size of the MT–pursuit direction correlation was present even before the onset of stimulus motion. We cannot attribute the relationship before the onset of stimulus motion to covariation of spontaneous activity with stimulus-driven response (mean $R = -0.01$, $p > 0.4$, one-sample *t* test), or to correlation of spontaneous activity with the MT–pursuit correlation for either direction (Spearman's $R = -0.01$ for direction, $p > 0.9$) or speed ($R = -0.08$, $p > 0.4$). Our initial conclusion, to be bolstered later in this article, is that the spike-field coherence is related to the correlation between the spike counts of pairs of neurons. Both are present during spontaneous activity as well as during stimulus-driven activity, and the size of the neuron–neuron correlation is related to the magnitude of the MT–pursuit correlation.

Spike-field coherence does not predict MT–pursuit correlation for eye speed

We performed the same analysis of the relationship between spike-field coherence and MT–pursuit correlations for eye speed as we did above for eye direction. We sorted the neurons in the population by the size of MT–pursuit speed correlation and selected the two groups of 20 neurons that showed the largest (mean $|R| = 0.19$) and smallest (mean $|R| = 0.02$) MT–pursuit speed correlations. Again, the two groups showed almost identical firing rate responses to stimulus motion (Fig. 5*C*), had the same overall power in the LFP (Fig. 5*D*), and had the same numbers of neurons from each of the two monkeys.

We observed smaller differences in the spike-field coherence between the two groups of neurons with high versus low values of MT–pursuit speed correlation, compared with the MT–pursuit direction correlation. For example, the traces in Figure 5*A* reveal statistically significant differences in spike-field coherence between the groups only in the 30–40 Hz frequency range (one-tailed Wilcoxon rank sum test, $p < 0.05$). Further, we had to use the spike trains in the interval from 20 to 120 ms after the onset of target motion to find significant differences. Similar, statistically significant effects were present for earlier intervals, but not for later intervals, including the 40–140 ms interval used for the analysis of MT–pursuit correlations for direction. Spike-triggered averaging of the LFPs did not reveal differences between the two groups of neurons in the frequency ranges from 10 to 30, 30–80, or 80–170 Hz. The summary of the correlations between the MT–pursuit speed correlations and the spike-field coherence confirms a relationship mainly for early times and for frequencies

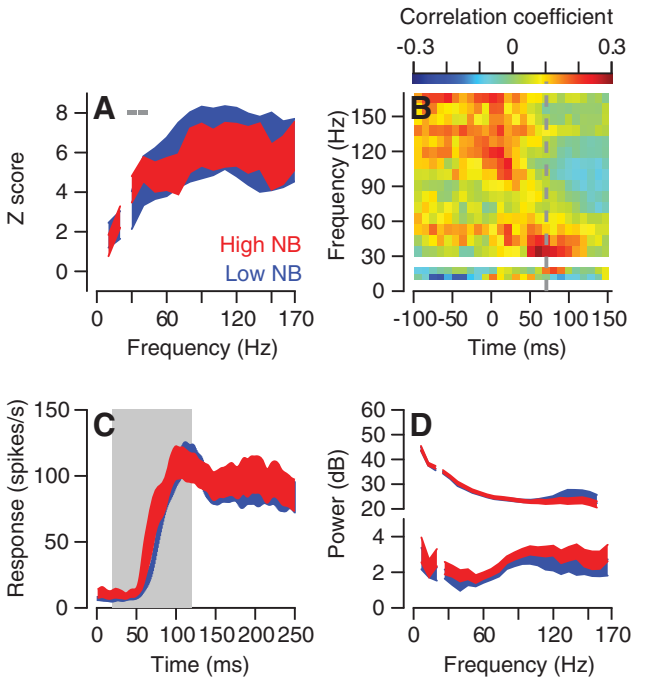

Figure 5. Relationship between LFPs and MT–pursuit correlation for speed. Red and blue ribbons show mean ± 1 SE for groups of 20 neurons with the highest and lowest amplitude MT–pursuit correlations. ***A***, Shuffle-corrected *z*-scores. Gray bars mark significant differences between the two groups (one-tailed Wilcoxon rank sum test, $p < 0.05$). ***B***, Correlation across all of the 96 neurons for shuffle-corrected *z*-scores versus MT–pursuit speed correlations. The color of each pixel shows the Spearman's *R* value for a given time point and frequency. The gray dashed line shows the time used for the group comparisons in ***A*** and ***C***. ***C***, Population average peristimulus time histograms. Gray-shaded area indicates the time epoch used for the spike-field coherence analysis in ***A***. ***D***, Upper and lower graphs in ***D*** show raw power spectrum and corrected power spectrum: spectrum of visual motion minus spectrum during fixation.

in the low gamma band (30–40 Hz; Fig. 5*B*). The relationship was present mainly in neurons with the lower half of MT–pursuit correlations for direction, but remained weak even in this group. Thus, spike-field coherence is slightly predictive of MT–pursuit correlations for eye speed, but is much more predictive of the MT–pursuit correlations for eye direction.

Spike-field coherence does not depend on behavioral conditions

In the analysis so far, we selected time windows for the analysis of spike-field coherence that were early enough in the stimulus to exclude any effects of feedback from changes in image motion caused by the initiation of pursuit. Also, we computed *z*-scores relative to shuffled data to exclude biases that could accompany transient responses in spikes and LFPs. As a further test of the relationship between spike-field coherence and MT–pursuit correlations, we also evaluated spike-field coherence during intervals when animals viewed a moving stimulus while fixating a stationary spot, using data obtained in the block of trials designed to characterize receptive field properties. Monkeys fixated a stationary spot while visual motion appeared in the receptive field of the neurons under study. Data obtained during fixation confirmed all the observations made during the initiation of pursuit.

As before, we selected the two groups of 20 neurons with the largest and smallest values of MT–pursuit correlation for direction; note that MT–pursuit correlation had to be assessed for each neuron from trials where the monkey tracked the moving stimulus. The average firing rate responses to the onset of stimulus motion during fixation were almost identical in the two groups (Fig. 6*A*), and tracking eye velocities were very small and delayed (Fig. 6*A*). The *z*-scored spike-field coherence was statistically and visibly higher for the neurons with the largest versus smallest values of MT–pursuit correlation for eye direction (Fig. 6*B*, compare red and blue traces). Again, the spike-field coherence in the gamma band was correlated positively with the MT–pursuit correlation for eye direction across the population of neurons studied during both pursuit initiation and fixation (Fig. 6*C*). The persistence of the relationship between spike-field coherence and MT–pursuit correlation for the entire duration of the time base in Figure 6*C* is expected given that the monkeys did not alter image motion by initiating pursuit. The persistence during the sustained component of MT responses obviates any concerns that the spike-field coherence might be a byproduct of transient responses in MT neurons.

Our findings are not a consequence of the small drifts of eye position that can be present during fixation, and that can affect the firing of MT neurons and their responses to stimulus motion (Bair and O'Keefe, 1998; Hohl and Lisberger, 2011). In monkey R, we stabilized image motion from the stimulus in a time window from 400 ms before to 126 ms after the onset of stimulus motion. Again, we divided the 53 neurons we tested with image stabilization into two groups of 10 neurons that showed the largest versus smallest MT–pursuit correlations for eye direction, and we evaluated the *z*-scored spike-field coherence for the two groups. The spike-field coherence in the gamma band was statistically larger in the group of neurons with the larger values of MT–pursuit correlation for eye direction (Fig. 7), and, if anything, the difference between the groups was slightly more pronounced for stimuli presented during image motion stabilization (Fig. 7*B*) than for stimuli during the pursuit of nonstabilized target motion (Fig. 7*A*).

Neuron–neuron correlation is related to spike-field coherence

We have shown so far that neurons whose spikes are synchronized statistically with the gamma frequency band of the LFP also have larger trial-by-trial correlations with the eye direction of pursuit. A prior study (Hohl et al., 2013) argued that MT–pursuit correlations emerge because of the neuron–neuron correlations between the spike counts of MT neurons that prefer similar stimuli (Huang and Lisberger, 2009). It follows that MT neurons with high spike-field coherence might have stronger correlations with their neighbors. We test this hypothesis next.

We analyzed the data for 39 pairs of MT neurons recorded while monkeys initiated pursuit eye movements. We start by showing the results for three pairs of neurons that had low, medium, and high values of neuron–neuron correlation at the onset of their responses to target motion ($R = 0.003, 0.09, 0.24$). When neurons in the pair had low correlations, both tended to have low spike-field coherence in the gamma-band frequency range (Fig. 8*A*,*D*). When neurons in the pair had high correlations, they tended to have high spike-field coherence in the gamma-band frequencies (Fig. 8*C*,*F*). Neuron–neuron correlations tended to be intermediate if one neuron had relatively high spike-field coherence while the other had low spike-field coherence (Fig. 8*B*,*E*). We summarized the spike-field coherence for each pair of neurons by multiplying the *z*-scores at each frequency, leading to curves with amplitudes that predicted the values of neuron–neuron correlation in the three example neurons (Fig. 8*G–I*).

We sorted the 39 pairs of neurons into two groups of NN neurons with the highest and lowest neuron–neuron correlations (mean $|R| = 0.22$ vs mean $|R| = 0.02$). Comparison of the product of the *z*-scores for spike-field coherence in the pairs for the two

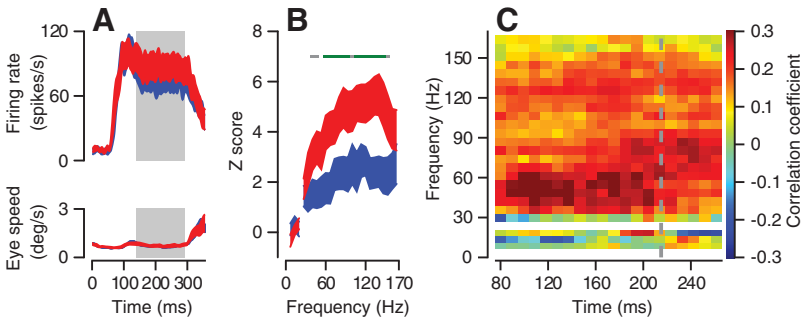

Figure 6. Spike-field coherence during visual motion with fixation. ***A***, Mean ± 1 SE of firing rate and eye speed in response to visual motion presented during fixation for groups of neurons with high (red) versus low (blue) MT pursuit-correlations. Shaded gray area marks the analysis window for spike-field coherence. ***B***, Comparison of shuffle-corrected *z*-scores. Green and gray bars at the top of the graph represent differences between the two groups that were statistically significant at $p < 0.01$ and $p < 0.05$ (one-tailed Wilcoxon rank sum test). ***C***, Correlations between shuffle-corrected *z*-scores and MT–pursuit direction correlations for all cells tested with visual motion during fixation. The color of each pixel shows the Spearman's *R* value for a given time point and frequency.

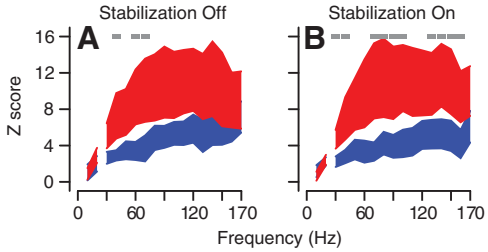

Figure 7. Spike-field coherences during pursuit without image stabilization (***A***) and with image stabilization (***B***). Red and blue ribbons show averages ± 1 SE for groups of MT neurons with high versus low MT–pursuit correlations for direction. Gray bars at the top of the graphs show frequencies where spike-field coherences were significantly larger for high-correlation versus low-correlation groups (one-tailed Wilcoxon rank sum test, $p < 0.05$). Data are from monkey R.

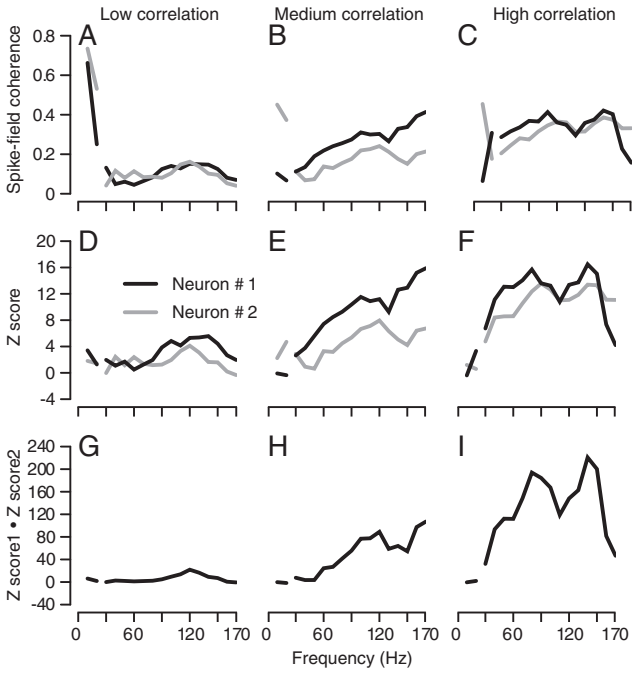

Figure 8. Example neuron pairs showing the relation between neuron–neuron correlation and spike-field coherence. ***A–C***, Spike-field coherence for each neuron in the pair. ***D–F***, Shuffle-corrected *z*-score for each neuron in the pair. ***G–I***, Product of the two shuffle-corrected *z*-scores in the pair. The three columns show pairs with low, medium, and high neuron–neuron correlations.

groups reveals larger coherence in the gamma band for the group with the larger values of neuron–neuron correlation (Fig. 9*B*, compare red, blue traces). The same result appeared in correlations across the full database of 39 pairs (Fig. 9*C*). As we noted before in similar analyses for other parameters, the relationship between the product of *z*-scores and neuron–neuron correlation is present before the onset of visual motion, at negative values of time in Figure 9*C*. We think this indicates that neuron–neuron correlation and spike-field coherence are present in spontaneous as well as driven activity. Finally, we verified that the relationship between the product of *z*-scores and the neuron–neuron correlation also is present when we grouped the pairs of neurons according to the product of *z*-scores rather than according to the magnitude of neuron–neuron correlation. We sorted the pairs by the product of the *z*-scores of spike-field coherence at 40 Hz, and selected the groups of 10 pairs with the highest and lowest *z*-score products. The neuron–neuron correlation was significantly larger in the high versus the low *z*-scores product group (0.17 ± 0.03 vs 0.06 ± 0.02, $p < 0.01$, two-tailed Wilcoxon rank sum test).

Usually, the two neurons within each pair preferred somewhat different stimulus speeds and direction, and we had to compute neuron–neuron correlations on the basis of responses to a single stimulus that was a good compromise between the preferences of the two neurons. Because neuron–neuron correlations depend on the similarity of preferred direction/speed for the pair of neurons (Huang and Lisberger, 2009), we asked whether preferred stimulus was a confounding factor in the relationship between neuron–neuron correlation and spike-field coherence. We tested the effect of preferred direction and speed differences within a pair on the relation between neuron–neuron correlation and spike-field coherence through partial correlation with differences of preferred direction or speed as control factors. The original correlation between the size of the neuron–neuron correlation and the product of *z*-scores at 40 Hz yielded a Spearman's $R = 0.43$ ($p < 0.05$). The results remained almost the same when we controlled direction preference differences ($R = 0.41$, $p < 0.05$) or speed preference differences ($R = 0.43$, $p < 0.05$). Therefore, we conclude that the spike-field coherence in the gamma frequency band is a predictor for neuron–neuron correlation, independent of similarities or differences in the preferred direction and speed of a pair of neurons.

Discussion

Correlated noise within a population of neurons places important constraints on how effectively sensory parameters can be estimated from a population response. Even weak correlations among the neural responses can cause a large population of neurons to act as if it were small, because pooling across neurons cannot reduce the correlated variation (Shadlen et al., 1996). As a result, the estimates of sensory parameters can be variable, and trial-by-trial variation in the discharge of individual neurons in the population might be correlated with the variation in the estimates derived through decoding. For example, when the same sensory stimulus is presented repeatedly, variation in responses of individual neurons in extrastriate visual area MT is informative

about variation in an impending perceptual decision (Britten et al., 1996) or the speed or direction of a visually guided eye movement (Hohl et al., 2013; this article).

Beyond the knowledge that some MT neurons are informative about the trial-by-trial variation in impending perceptual and motor behavior, the next fundamental question is about the meaning of the wide variation in how well different MT neurons predict the trial-by-trial variation in behaviors. It is tempting to average across neurons, under the assumption that we are dealing with small effects that would emerge from noise in only a fraction of neurons. However, it is equally likely that the differences among neurons reveal something fundamental about how neuron–behavior correlations emerge, or about the relative impact of different neurons on perceptual or motor behavior. We focus on the possibility that the variation across neurons is meaningful.

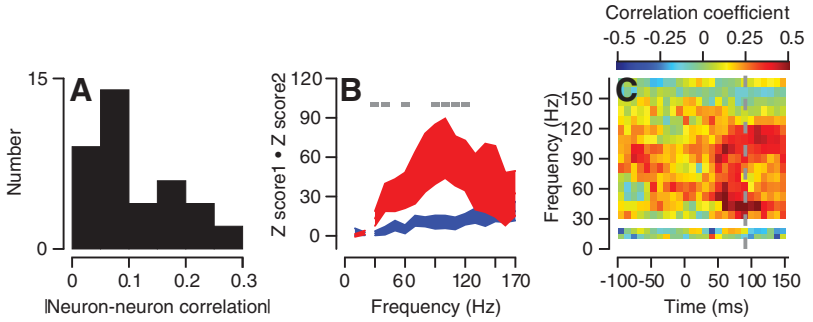

Figure 9. Population summary of the relation between neuron–neuron correlation and spike-field coherence. ***A***, Distribution of neuron–neuron correlation for 39 pairs. ***B***, Red and blue ribbons show the product of the spike-field coherence *z*-scores for groups of neuron pairs with high versus low neuron–neuron correlations. Gray bars at the top of the graph mark frequencies with significant difference between the two groups. ***C***, Correlations across all the 39 pairs for multiplication of *z*-scores versus neuron–neuron correlation. The color of each pixel shows the Spearman's *R* values for a given time point and frequency. Gray dotted line shows the time used for the group comparison in ***B***.

We found that the size of the MT–pursuit direction correlation is related to the strength of synchronization between individual action potentials and the gamma-band component of the LFP. If a neuron's spikes synchronized with the gamma-band frequency range of the LFP, then the trial-by-trial variation in its firing rate also correlated with variation in pursuit direction and with the firing of neighboring neurons. These results lead us to suggest that (1) different groups of neurons have different degrees of noise correlations with their neighbors, (2) noise correlations with other neurons are reflected in gamma-band oscillations in the LFP, and (3) neurons that have larger noise correlations with their neighbors also are better correlated with the decoded estimate of target direction. The last of these conclusions is based on the well documented likelihood that the first 100 ms of pursuit is a valid probe for the result of population decoding of target direction (Lisberger and Westbrook, 1985; Osborne et al., 2005).

Other possible causes of spike-field coherence

Several of our observations argue against the possibility that visual inputs caused by small eye movements during fixation could, as a common input, induce coherence between the spikes of MT neurons and LFPs (Hohl and Lisberger, 2011). First, the drifts during fixation have peak power at a frequency of ~5 Hz, but we did not see a significant relationship between MT–pursuit correlations and the low-frequency LFP. Second, the effects reported here weathered partial correlation analysis, ruling out an effect of eye movements that happens in advance of the time window for spike count. Third, our results persisted when we stabilized image motion on the retina. If MT responses evoked by the drifts of fixation had created the MT–pursuit correlation and spike-field coherence in the gamma band, then the effects we have reported should have vanished under image stabilization.

Because we recorded spikes and LFP from the same electrode, our conclusions could depend on cross talk ("spike bleed-through") between spikes and the LFPs (Ray and Maunsell, 2011). However, some aspects of our data argue against this possibility. First, our results persist even after we have excised a portion of LFPs at the time of each spike (see Materials and Methods). Second, the relationship between spike-field coherence and MT–pursuit correlations appears at fairly low gamma frequencies (from ~30 Hz) and decreases at high gamma frequencies (>120 Hz). If the effects were dominated by spike bleed-through, then they should be largest in the high gamma band. Third, we did not see significant differences in the power of the LFP at a given site as a function of MT–pursuit correlation of neurons recorded at that location; the analysis by Ray and Maunsell (2011) implies that there should have been a difference if our findings about spike-field coherence are due to bleed-through. Finally, the relationship between MT–pursuit correlation and spike-field coherence argue that the spike-field coherence in our measurements cannot be attributed solely to the spike bleed-through. There is no reason to think that neurons at sites with stronger spike bleed-through would have stronger correlations with pursuit behavior.

We also think that the relationship between the MT–pursuit correlation and the spike-field coherence does not depend on variation across sessions in stimulus properties that affect the gamma rhythm, such as contrast (Henrie and Shapley, 2005; Ray and Maunsell, 2010), orientation (Jia et al., 2011), target direction and speed (Liu and Newsome, 2006), and stimulus size (Gieselmann and Thiele, 2008; Jia et al., 2011; Ray and Maunsell, 2011). Contrast is not a concern because we did not change stimulus luminance across sessions. The direction and speed of visual motion and the size of the stimulus varied across recording sessions to match stimulus properties to the preferred stimuli of the neurons under study. However, none of these stimulus parameters varied significantly between the groups of neurons with high versus low magnitudes of MT–pursuit correlation, and high versus low spike-field coherences in the gamma band.

The meaning of heterogeneous neuronal populations defined by the degree of gamma synchrony

Several neural mechanisms might explain the relationship we found between spike-field coherence in the gamma band and MT–pursuit correlations, as follows: (1) stronger neuron–neuron correlations cause both larger spike-field coherence and larger MT–pursuit correlations; (2) coherence of spikes with the gamma rhythm might endow the spikes with more powerful influences on downstream circuits, leading to larger MT–pursuit correlations; and (3) neurons with larger MT–pursuit correlations might have stronger output connections and also happen to reside in cortical layers where neurons have stronger spike-field coherences through separate mechanisms.

We favor the first explanation. We think that gamma-band spike-field coherence is an unavoidable side-effect of mechanisms that lead to high correlations among neighboring neurons (Jia et al., 2013), and that large neuron–neuron correlations create large MT–pursuit correlations. This explanation is compatible with the differences in our results for MT–pursuit correlations along the axes of eye direction versus speed. The grouping of MT neurons into direction columns might promote spike-field coherence based on correlations with neighboring neurons having the same preferred direction. The weaker organization for preferred speed in MT (Liu and Newsome, 2003) might allow a neuron to have a high MT–pursuit correlation even though the topographical spread of the correlated neurons would work against a high value of spike-field coherence.

Others have suggested that the gamma rhythm could have a causal role in enhancing cognitive functions such as attention (Fries et al., 2001; Womelsdorf et al., 2006; Gregoriou et al., 2009; Bosman et al., 2012), memory formation (Jutras et al., 2009), decision making (Donner et al., 2009), and working memory (Pesaran et al., 2002). Some studies have suggested that gamma rhythm plays an important role in basic sensory processes such as orientation selectivity (Womelsdorf et al., 2012) and response normalization (Ray et al., 2013). At an extreme, our data could be taken as support for the idea that gamma synchrony facilitates transmission of information among different brain areas (Schoffelen et al., 2005; Gregoriou et al., 2009; Bosman et al., 2012; Roberts et al., 2013), causing specific MT neurons to have a larger impact on the behavioral output and, therefore, to have larger values of MT–pursuit correlation. However, we do not favor this explanation, mainly because simpler mechanisms that are known to exist can explain our findings.

Neurons in the output layers of MT might have the strongest neuron–behavior correlations because they have the strongest connections to downstream circuits. Indeed, neurons in supragranular layers of the visual cortex have stronger neuron–neuron correlations than do neurons in input layers (Hansen et al., 2012; Smith et al., 2013), and also show stronger synchrony with gamma-band LFPs (Buffalo et al., 2011). If the same situation holds in area MT, then neurons in the output layers would be expected to have the largest values of neuron–neuron correlation and MT–pursuit correlation, but for separate and independent reasons. We think that the absence of a relationship between MT–pursuit correlations for direction and speed argues against a causal role for the strength of output connections in determining the size of MT–pursuit correlations, because it separates the size of the MT–pursuit correlation, which are unrelated within a given neuron, from the strength of the output connections, which are a fixed property of each neuron. Thus, a neuron that lacks MT–pursuit correlation could still play a key role in driving pursuit behavior, but, because it lacks correlations with its near neighbors, it would not show a "noise" correlation with the trial-by-trial variation in behavior. At the same time, strong correlations with neurons that drive behavior might allow a neuron to show large MT–pursuit correlations even if it lacks physical connections to the circuits that drive behavior (Cohen and Newsome, 2008; Nienborg and Cumming, 2010; Bosking and Maunsell, 2011).

In conclusion, our data and prior research lead us to suggest that spike-field coherence in the gamma band is an index of correlated variation among neighboring neurons. Neuron–neuron correlations cause variation in the firing of individual neurons to be correlated with the estimates of sensory parameters obtained by decoding the population (Zohary et al., 1994; Shadlen et al., 1996; Hohl et al., 2013). Larger correlations with its neighbors cause a neuron to have a larger MT–pursuit correlation.

References

Bair W, Koch C (1996) Temporal precision of spike trains in extrastriate cortex of the behaving macaque monkey. Neural Comput 8:1185–1202. CrossRef Medline

Bair W, O'Keefe LP (1998) The influence of fixational eye movements on the response of neurons in area MT of the macaque. Vis Neurosci 15:779–786. Medline

Berens P, Logothetis NK, Tolias AS (2012) Local field potentials, BOLD and spiking activity: relationships and physiological mechanisms. In: Visual population codes—towards a common multivariate framework for cell recording and functional imaging (Kriegeskorte N, Kreiman G, eds), pp 599–624. Cambridge, MA: MIT.

Bokil H, Purpura K, Schoffelen JM, Thomson D, Mitra P (2007) Comparing spectra and coherences for groups of unequal size. J Neurosci Methods 159:337–345. CrossRef Medline

Bokil H, Andrews P, Kulkarni JE, Mehta S, Mitra PP (2010) Chronux: a platform for analyzing neural signals. J Neurosci Methods 192:146–151. CrossRef Medline

Bosking WH, Maunsell JH (2011) Effects of stimulus direction on the correlation between behavior and single units in area MT during a motion detection task. J Neurosci 31:8230–8238. CrossRef Medline

Bosman CA, Schoffelen JM, Brunet N, Oostenveld R, Bastos AM, Womelsdorf T, Rubehn B, Stieglitz T, De Weerd P, Fries P (2012) Attentional stimulus selection through selective synchronization between monkey visual areas. Neuron 75:875–888. CrossRef Medline

Britten KH, Newsome WT, Shadlen MN, Celebrini S, Movshon JA (1996) A relationship between behavioral choice and the visual responses of neurons in macaque MT. Vis Neurosci 13:87–100. CrossRef Medline

Buffalo EA, Fries P, Landman R, Buschman TJ, Desimone R (2011) Laminar differences in gamma and alpha coherence in the ventral stream. Proc Natl Acad Sci U S A 108:11262–11267. CrossRef Medline

Buracas GT, Zador AM, DeWeese MR, Albright TD (1998) Efficient discrimination of temporal patterns by motion-sensitive neurons in primate visual cortex. Neuron 20:959–969. CrossRef Medline

Cohen MR, Newsome WT (2008) Context-dependent changes in functional circuitry in visual area MT. Neuron 60:162–173. CrossRef Medline

Donner TH, Siegel M, Fries P, Engel AK (2009) Buildup of choice-predictive activity in human motor cortex during perceptual decision making. Curr Biol 19:1581–1585. CrossRef Medline

Fries P, Reynolds JH, Rorie AE, Desimone R (2001) Modulation of oscillatory neuronal synchronization by selective visual attention. Science 291:1560–1563. CrossRef Medline

Gieselmann MA, Thiele A (2008) Comparison of spatial integration and surround suppression characteristics in spiking activity and the local field potential in macaque V1. Eur J Neurosci 28:447–459. CrossRef Medline

Gregoriou GG, Gotts SJ, Zhou H, Desimone R (2009) High-frequency, long-range coupling between prefrontal and visual cortex during attention. Science 324:1207–1210. CrossRef Medline

Haefner RM, Gerwinn S, Macke JH, Bethge M (2013) Inferring decoding strategies from choice probabilities in the presence of correlated variability. Nat Neurosci 16:235–242. CrossRef Medline

Hansen BJ, Chelaru MI, Dragoi V (2012) Correlated variability in laminar cortical circuits. Neuron 76:590–602. CrossRef Medline

Henrie JA, Shapley R (2005) LFP power spectra in V1 cortex: the graded effect of stimulus contrast. J Neurophysiol 94:479–490. CrossRef Medline

Hohl SS, Lisberger SG (2011) Representation of perceptually invisible image motion in extrastriate visual area MT of macaque monkeys. J Neurosci 31:16561–16569. CrossRef Medline

Hohl SS, Chaisanguanthum KS, Lisberger SG (2013) Sensory population decoding for visually guided movements. Neuron 79:167–179. CrossRef Medline

Huang X, Lisberger SG (2009) Noise correlations in cortical area MT and their potential impact on trial-by-trial variation in the direction and speed of smooth-pursuit eye movements. J Neurophysiol 101:3012–3030. CrossRef Medline

Jarvis MR, Mitra PP (2001) Sampling properties of the spectrum and coherency of sequences of action potentials. Neural Comput 13:717–749. CrossRef Medline

Jia X, Smith MA, Kohn A (2011) Stimulus selectivity and spatial coherence of gamma components of the local field potential. J Neurosci 31:9390–9403. CrossRef Medline

Jia X, Tanabe S, Kohn A (2013) Gamma and the coordination of spiking activity in early visual cortex. Neuron 77:762–774. CrossRef Medline

Jutras MJ, Fries P, Buffalo EA (2009) Gamma-band synchronization in the macaque hippocampus and memory formation. J Neurosci 29:12521–12531. CrossRef Medline

Katzner S, Nauhaus I, Benucci A, Bonin V, Ringach DL, Carandini M (2009) Local origin of field potentials in visual cortex. Neuron 61:35–41. CrossRef Medline

Krauzlis RJ (2003) Neuronal activity in the rostral superior colliculus related to the initiation of pursuit and saccadic eye movements. J Neurosci 23:4333–4344. Medline

Le Digabel S (2011) Algorithm 909: NOMAD: nonlinear optimization with the MADS algorithm. ACM Trans Math Softw 37:1–15. CrossRef

Lisberger SG, Westbrook LE (1985) Properties of visual inputs that initiate horizontal smooth pursuit eye movements in monkeys. J Neurosci 5:1662–1673. Medline

Liu J, Newsome WT (2003) Functional organization of speed tuned neurons in visual area MT. J Neurophysiol 89:246–256. Medline

Liu J, Newsome WT (2006) Local field potential in cortical area MT: stimulus tuning and behavioral correlations. J Neurosci 26:7779–7790. CrossRef Medline

Medina JF, Lisberger SG (2007) Variation, signal, and noise in cerebellar sensory-motor processing for smooth-pursuit eye movements. J Neurosci 27:6832–6842. CrossRef Medline

Mitra PP, Pesaran B (1999) Analysis of dynamic brain imaging data. Biophys J 76:691–708. CrossRef Medline

Mitzdorf U (1985) Current source-density method and application in cat cerebral cortex: investigation of evoked potentials and EEG phenomena. Physiol Rev 65:37–100. Medline

Morris EJ, Lisberger SG (1987) Different responses to small visual errors during initiation and maintenance of smooth-pursuit eye movements in monkeys. J Neurophysiol 58:1351–1369. Medline

Nienborg H, Cumming BG (2006) Macaque V2 neurons, but not V1 neurons, show choice-related activity. J Neurosci 26:9567–9578. CrossRef Medline

Nienborg H, Cumming B (2010) Correlations between the activity of sensory neurons and behavior: how much do they tell us about a neuron's causality? Curr Opin Neurobiol 20:376–381. CrossRef Medline

Osborne LC, Lisberger SG (2009) Spatial and temporal integration of visual motion signals for smooth pursuit eye movements in monkeys. J Neurophysiol 102:2013–2025. CrossRef Medline

Osborne LC, Lisberger SG, Bialek W (2005) A sensory source for motor variation. Nature 437:412–416. CrossRef Medline

Palmer C, Cheng SY, Seidemann E (2007) Linking neuronal and behavioral performance in a reaction-time visual detection task. J Neurosci 27:8122–8137. CrossRef Medline

Pesaran B, Pezaris JS, Sahani M, Mitra PP, Andersen RA (2002) Temporal structure in neuronal activity during working memory in macaque parietal cortex. Nat Neurosci 5:805–811. CrossRef Medline

Ramachandran R, Lisberger SG (2005) Normal performance and expression of learning in the vestibulo-ocular reflex (VOR) at high frequencies. J Neurophysiol 93:2028–2038. Medline

Ray S, Maunsell JH (2010) Differences in gamma frequencies across visual cortex restrict their possible use in computation. Neuron 67:885–896. CrossRef Medline

Ray S, Maunsell JH (2011) Different origins of gamma rhythm and high-gamma activity in macaque visual cortex. PLoS Biol 9:e1000610. CrossRef Medline

Ray S, Ni AM, Maunsell JH (2013) Strength of gamma rhythm depends on normalization. PLoS Biol 11:e1001477. CrossRef Medline

Roberts MJ, Lowet E, Brunet NM, Ter Wal M, Tiesinga P, Fries P, De Weerd P (2013) Robust gamma coherence between macaque V1 and V2 by dynamic frequency matching. Neuron 78:523–536. CrossRef Medline

Schoffelen JM, Oostenveld R, Fries P (2005) Neuronal coherence as a mechanism of effective corticospinal interaction. Science 308:111–113. CrossRef Medline

Schoppik D, Nagel KI, Lisberger SG (2008) Cortical mechanisms of smooth eye movements revealed by dynamic covariations of neural and behavioral responses. Neuron 58:248–260. CrossRef Medline

Shadlen MN, Britten KH, Newsome WT, Movshon JA (1996) A computational analysis of the relationship between neuronal and behavioral responses to visual motion. J Neurosci 16:1486–1510. Medline

Smith MA, Jia X, Zandvakili A, Kohn A (2013) Laminar dependence of neuronal correlations in visual cortex. J Neurophysiol 109:940–947. CrossRef Medline

Snyder LH, Dickinson AR, Calton JL (2006) Preparatory delay activity in the monkey parietal reach region predicts reach reaction times. J Neurosci 26:10091–10099. CrossRef Medline

Womelsdorf T, Fries P, Mitra PP, Desimone R (2006) Gamma-band synchronization in visual cortex predicts speed of change detection. Nature 439:733–736. CrossRef Medline

Womelsdorf T, Lima B, Vinck M, Oostenveld R, Singer W, Neuenschwander S, Fries P (2012) Orientation selectivity and noise correlation in awake monkey area V1 are modulated by the gamma cycle. Proc Natl Acad Sci U S A 109:4302–4307. CrossRef Medline

Zohary E, Shadlen MN, Newsome WT (1994) Correlated neuronal discharge rate and its implications for psychophysical performance. Nature 370:140–143. CrossRef Medline